

## Chapter 7

# Transport in $\text{Cu}_2\text{Se}$ and $\text{Cu}_{1.97}\text{Ag}_{0.03}\text{Se}$

In the previous chapter I introduced super-ionic materials and band structure modeling of thermoelectrics. In that context I introduced the thermoelectric super-ionic material  $\text{Ag}_2\text{Se}$ , and in analyzing its transport I noted an increase in its Seebeck in its ordered phase compared to its disordered phase that appeared directly responsible for an increase in its thermoelectric performance. This change in its Seebeck coefficient was not explained with the band structure models typically used to explain thermoelectric transport.

In this chapter I will discuss  $\text{Cu}_2\text{Se}$ , which also shows an unexplained increase in its Seebeck and  $zT$  at its phase transition. In chapter 5 I noted that  $\text{Cu}_2\text{Se}$  shows a second order transition while  $\text{Ag}_2\text{Se}$  shows a first order transition. Its phase transition thermoelectric behavior reflects that characteristic. Before I discuss the transport behavior of  $\text{Cu}_2\text{Se}$  and  $\text{Cu}_{1.97}\text{Ag}_{0.03}\text{Se}$  I will introduce the concept of coupled entropy transport; this concept can be used to explain the behavior of these materials which will be done in detail in the concluding chapter.

### 7.1 Entropy and Charge Transport

A thermoelectric material is treated as having two principle interacting thermodynamic quantities: heat and electron current [31]. The equilibrium thermodynamics

of such a system are described by:

$$dS = \frac{1}{T}dU - \frac{\tilde{\mu}}{T}dN, \quad (7.1)$$

in which  $S$  and  $U$  are the entropy and internal energy of the system and  $N$  is the number of particles (carriers). Though I will address this part of my analysis in terms of these extensive quantities, it is often convenient to use the corresponding intensive quantities of entropy density ( $s$ ), energy density  $u$ , and carrier concentration ( $n$ ). Conversion from extensive to intensive quantities in these formulations is simply a matter of substituting the intensive variable for an extensive variable.

The nature of an irreversible process is that it produces entropy. A thermodynamic formulation in which the extensible quantities are expressed as differentials, as in Equation 7.1, will have a simple equivalent in irreversible thermodynamics. The entropy production associated with a linear process is: Equation 7.1 is [32]:

$$\dot{S} = \nabla \frac{1}{T} \cdot J_U - \nabla \frac{\tilde{\mu}}{T} \cdot J_N, \quad (7.2)$$

in which the  $J_x$  are thermodynamic fluxes and the gradient terms are thermodynamic affinities. Under a given set of boundary condition, *i.e.*, a particular resistor acting as a load and under steady state, the systems properties will be arranged such that  $\dot{S}$  is minimized. This theoretical result is known as the minimum entropy principle. Of course  $\dot{S}$  is always greater than or equal to zero, or else the second law of thermodynamics would be violated. The ratio of the second term in Equation 7.2 to its first terms describes the reversibility of the heat engine. When the load is varied to maximize that ratio, that maximal value is  $zT$ .

On the micro-foundation of the fluctuation-dissipation theorem Onsager proved that thermodynamics forces and fluxes associated in entropy production could be related linearly [147]. Generally:

$$\begin{bmatrix} J_1 \\ J_2 \end{bmatrix} = - \begin{bmatrix} L_{11} & L_{12} \\ L_{21} & L_{22} \end{bmatrix} \begin{bmatrix} \nabla X_1 \\ \nabla X_2 \end{bmatrix} \quad (7.3)$$

The  $L_{xy}$  are known as the Onsager coefficients and they may depend on any set of thermodynamic quantities that describe the system. By the Onsager reciprocity theorem  $L_{12} = L_{21}$ . For the specific case of thermoelectricity:

$$\begin{bmatrix} J \\ J_S \end{bmatrix} = - \begin{bmatrix} L_{ee} & L_{es} \\ L_{se} & L_{ss} \end{bmatrix} \begin{bmatrix} \nabla V \\ \nabla T \end{bmatrix} \quad (7.4)$$

Here I use entropy transport instead of heat transport to avoid the confusion between the two different definitions of heat flux commonly used [49]. The Callen heat flux  $Q \equiv TJ_s$  describes the heat transport through the material, while the DeGroot heat flux  $J_q \equiv \mu J_e + TJ_s$  describes that transporting from one heat reservoir to another [132]. In the case of thermoelectrics that distinction does not lead to any difference in description of the Onsager coefficients [49].

The Onsager coefficients may be related to  $\sigma, \alpha$ , and  $\kappa$  by:

$$\alpha = -\frac{L_{es}}{L_{ee}} \quad (7.5)$$

$$\sigma = L_{ee} \quad (7.6)$$

$$\kappa = T \left( \frac{L_{ee}L_{ss}L_{es}^2}{L_{ee}} \right) \quad (7.7)$$

While ideal for describing the macroscopic relations between the phenomenological transport coefficients, the irreversible thermodynamics of the Onsager relations cannot actually produce the values of those coefficients. The kinetic theory approach is therefore preferred for understanding how chemical structure, bands structure, and doping give the values of these coefficients. For this the Boltzmann transport equation is used:

$$\frac{\partial f}{\partial T} = \left( \frac{\partial f}{\partial T} \right)_{force} + \left( \frac{\partial f}{\partial T} \right)_{diff} + \left( \frac{\partial f}{\partial T} \right)_{coll} \quad (7.8)$$

Here  $f$  is the electron state occupation probability density. When eq (7.8) is solved

it will generally have the form given by Kubo [112, 113]:

$$q\alpha = -\frac{\mu}{T} - k_b T \frac{M_{qe}}{M_{ee}} \quad (7.9)$$

$M_{qe}$  and  $M_{ee}$  are transport integrals representing heat transport per electron and current transported per electron. A comparable expression may be derived from only non-equilibrium thermodynamics considerations [49].

$$\alpha \equiv \frac{-\mu}{T} + \frac{1}{qT} J_q \quad (7.10)$$

From comparison with Equation 7.10, we see that Equation 7.9 is actually the sum of two separate thermodynamic transport quantities. The first term represents the entropy transport due to the change in the number of carrier present. It is the thermodynamic equivalent of heat transport by mass flow in a liquid-based heat exchanger. Following Emin [61], we refer to the first term as the presence Seebeck,  $\alpha_{presence}$ . The presence Seebeck is convenient to work with because it can be expressed entirely in terms of equilibrium thermodynamics:

$$\alpha_{presence} \equiv -\frac{\mu}{qT} \equiv \frac{1}{q} \left( \frac{\partial S}{\partial n} \right)_U \quad (7.11)$$

The second term in Equations 7.9,7.10 represents the part of the Seebeck that results from the manner in which charge is transported. It reflects contribution from the scattering interaction of the moving heat and charge and the distortion transport effects on the state occupations and energies. For this reason, again following Emin, we refer to it as the transport portion of Seebeck,  $\alpha_{transport}$ . [61] Solving for  $\alpha_{transport}$  exactly would require a perfect understanding of all electron scattering mechanisms and the band structure, and its determination is the primary focus of band structure modeling.

## 7.2 Entropy Co-Transport

In the discussion in section 7.1 above we implicitly assumed that the only thermodynamic quantities that transported were charge and entropy. While the formulations of eqs.7.4,7.9 are completely phenomenological and general, calculating the Onsager coefficients under this assumption will lead to a discrepancy with measurement. The entropy associated with co-transport of the non-electronic thermodynamic flux will be attribute to  $\alpha_{transport}$ ; however, the transport calculations based on a static band structure will be unable to replicate that effect.

To include the effect of another thermodynamic variable, I first add an additional term to equation 7.1.

$$dS = \frac{1}{T}dU - \frac{\tilde{\mu}}{T}dN + hdm \quad (7.12)$$

There will be a thermodynamic flux ( $J_m$ ) associated with  $m$  and a thermodynamic force ( $\nabla h$ ) associated with  $h$ . If a flux of electrons drags a flux of  $m$ , then that the entropy transported per carrier should be enhanced by the presence entropy of those units of  $m$ . The presence entropy is then:

$$\alpha_{presence} = \frac{1}{q} \left( \frac{\partial S}{\partial n} \right)_U + \frac{1}{q} \left( \frac{\partial S}{\partial m} \right)_{U,N} \left( \frac{\partial m}{\partial n} \right)_{U,S} \quad (7.13)$$

In chapter 8 this relation will be motivated from non-equilibrium thermodynamics.

Entropy co-transport enhancements to Seebeck and  $zT$  have been observed in several material systems. Aselage *et. al* [7] determined  $B_{12+x}C_{3-x}4$ ,  $0.15 < x < 1.7$  to have a Seebeck coefficient of  $\approx 200\mu V/K$  despite a carrier concentration of  $\approx 10^{21} \text{ cm}^{-3}$ . A Seebeck coefficient of  $10 \mu V/K$  would be expected at such a high carrier concentration. In this material carriers transport as polarizable pairs, called *bipolarons*. The presence of these bipolarons modifies by a dipole interaction atomic vibrational frequencies [62]. By modeling the entropy contribution associated with this bipolaron mode softening, Emin was able to explain the behavior of these Boron Carbides as due to phonon entropy co-transport [61] Such vibrational softening enhancements of Seebeck are referred to as phonon drag Seebeck effects, and they have

been observed in other systems [39, 11, 10].

By coupling the spin degree of freedom to entropy transport, increased Seebeck in  $\text{Na}_x\text{CoO}_2$  has been shown [196, 110, 139]. The differing spin degeneracy of electron-occupied and electron-unoccupied cobalt sites provides the mechanism for this coupling of carrier transport to entropy transport [138]. Here we consider coupling the carrier transport to degrees of freedom associated with the structural changes of a phase transition. A phase transition is always associated with an entropy change because there is always a concurrent transformation in system symmetries [162]. In continuous (*i.e.*, second order) phase transitions the entropy will change over an extended temperature range. In chapter 5, we found the phase transition of  $\text{Cu}_2\text{Se}$  to have a substantially elevated heat capacity over a wide temperature range. If some part of the entropy associated with the phase transition is coupled to transport, a large Seebeck enhancement may be possible.

### 7.3 $\text{Cu}_2\text{Se}$ Transport near the Phase Transition

Copper (I) selenide is a p-type semiconductor [54]. Above 410 K  $\text{Cu}_2\text{Se}$  becomes super-ionic, which is characterized by its disordered  $\text{Cu}^+$  ions, and shows good thermoelectric properties [122]. Except at the highest temperatures, charge transport is dominated by holes rather than  $\text{Cu}^+$  ions. As the temperature drops below 410 K the ion mobility decreases [84] and eventually the Cu ions become ordered [96]. It is known that copper (I) selenide can be copper deficient ( $\text{Cu}_{2-\delta}\text{Se}$ ) with copper vacancies, and this has a large effect on transport properties and the phase structure [194].

Horvatic *et al.* showed that the ion conductivity of  $\text{Cu}_{1.99}\text{Se}$ s increases from 1 S/m at 374 K to almost 100 S/m at 410 K [84], demonstrating it to have a super-ionic phase transition. Below 374 K and above 410 K, he found that the ion conductivity followed an Arrhenius law with  $E_A = 0.29$  eV and  $E_A = 0.07$  eV, respectively. Each of these temperatures had been previously identified as corresponding to a phase transition in  $\text{Cu}_{2-\delta}\text{Se}$  ( $\delta < 0.045$ ) [194, 177]. In the intermediate temperature range, the ion conductivity changed rapidly. This behavior is indicative of a continuous phase

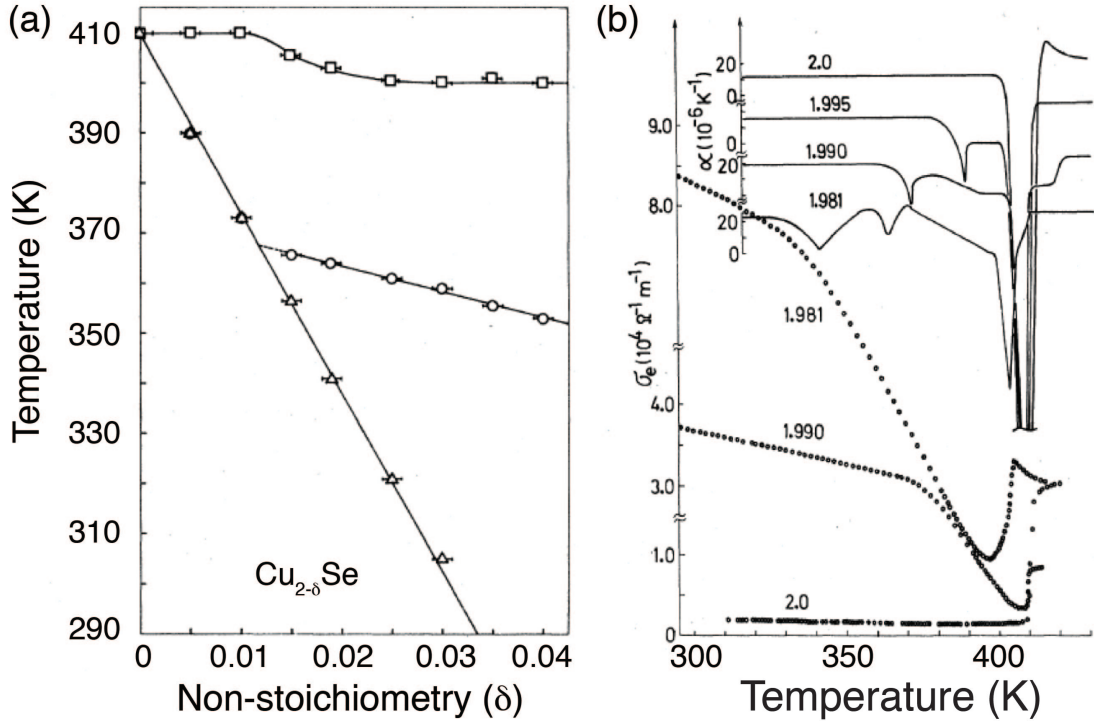


Figure 7.1: Phase diagram (a) determined by Vucic [194] on the basis of dilatometry (b) measurements. Adapted from Vucic *et al.* [192].

transition in a super-ionic material [21, 118]. An observation of not only structural entropy change at the phase transition but also of structural entropy transport is given by Korzhuev and Laptev [107]; they measured a sharp peak in the thermodiffusion of  $\text{Cu}^0$  in  $\text{Cu}_2\text{Se}$  at the 410 K phase transition. From this they calculated a heat of transport of Cu atoms of 1 eV.

Unusual transport effects have been observed before near the critical temperature in  $\text{Cu}_2\text{Se}$  [54, 122, 143, 144, 123, 200, 27], however, this is the first work that also considers changes in all thermal transport measurements ( $D_t, \kappa, c_p$ ) to derive an improved value for  $zT$ . Liu *et al.* report a  $zT$  greater than 1 [121], however their work assumes all the heat released as measured by DSC is due to a first order structural transformation. In that case it would be appropriate, as is done by Liu *et al.*, to calculate  $\kappa$  and  $zT$  using the smaller Delong-Petit heat capacity. As discussed in detail in chapter 5 the elevated peak in calorimetry is an equilibrium rather than kinetic aspect of the system behavior and must be used to determine  $zT$ .

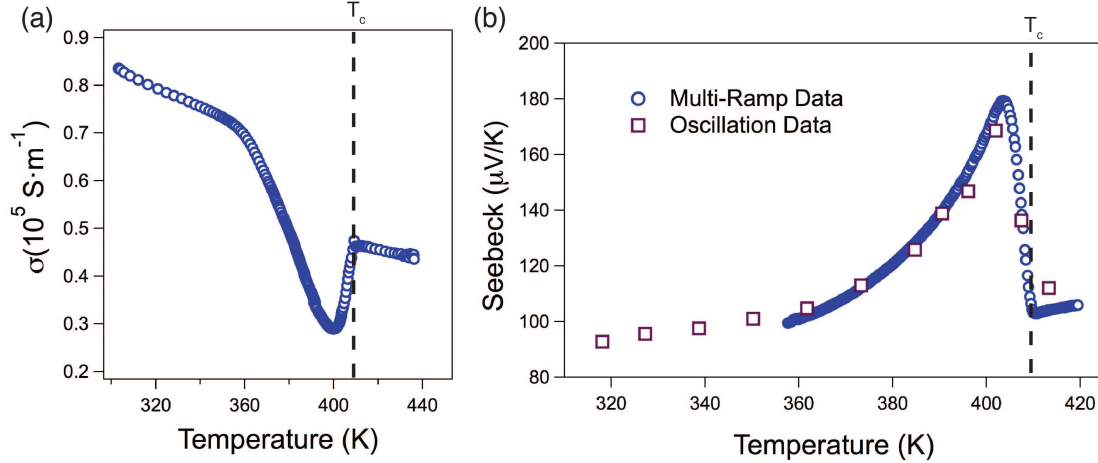


Figure 7.2: Electrical conductivity (a) and Seebeck Coefficient (b) measured through the 410K phase transition.

The study of electrical transport near the phase transition of  $\text{Cu}_{2-\delta}\text{Se}$  owes mostly to the work of Zlatko Vucic and his collaborators at the University of Zagreb [84, 194, 192, 191, 134, 193]. His measurements spanned the  $\delta = 0$  to  $\delta = 0.045$  single phase range [106]. Based on dilatometric measurements he developed a phase diagram for  $\text{Cu}_{2-\delta}\text{Se}$ , see Figure 7.1. At all compositions he found a phase transition at  $\approx 410$  K and a second phase transition at a lower temperature with temperature dependent on  $\delta$ . The data presented on the sample of  $\text{Cu}_2\text{Se}$  presented here corresponds generally to his observations of his  $\delta = 0.01$  sample. WDS data on  $\text{Cu}_2\text{Se}$  bounded  $\delta < 0.005$  for this sample; the reason for this disagreement is unclear.

Electrical conductivity (Figure 7.2(a)) was measured at a heating rate of 10 K/hr. It shows three main features: a knee at 355 K, a minimum at 400 K, and a kink at 410 K. The kink at 410 K corresponds to the observed phase transition in my crystallography data (section 5.3). In general shape  $\sigma(T)$  strongly resembles the data in Vucic's studies (Figure 7.1), though it corresponds best to his  $\text{Cu}_{1.99}\text{Se}$  stoichiometric sample.

The knee in conductivity at  $T_{c2} = 355$  K corresponds to the lower temperature second order phase transition measured by Vucic [192]. He empirically determined a

power law for  $\sigma$  below  $T_{c2}$ :

$$\sigma = \sigma_0 \left( 1 - \frac{T}{T_{c2}} \right) \quad (7.14)$$

From the low temperature slope a predicted  $T_c = 360$  K was determined, which is consistent with the  $T_{c2}$  determined by inspection. Above the phase transition the conductivity is again linear, though 20% lower than the value predicted by extrapolation from the low temperature behavior.

Seebeck was measured first by the standard oscillation method as described in chapter 3, see Figure 7.2(b). This showed a clear peak in the Seebeck, but the rapid non-linear change raised clear questions about the accuracy of those results. For this reason the ramp Seebeck approach was developed as described in chapter 3, allowing for detail temperature-resolved measurement of Seebeck through the phase transition. The three significant features observed in  $\sigma$  are echoed in  $\alpha$ . There is a kink in the Seebeck at 410 K, corresponding to the main phase transition observed in crystallography. Below 360 K  $\alpha$  is a linear function of temperature; above it shows non-linear behavior. There is a maxima in  $\alpha$  at 403 K, at a slightly elevated temperature compared to the 400 K minima in electrical conductivity. Above the phase transition the Seebeck is locally linear, though 10% lower than the value predicted by extension of the low temperature trend.

Thermal conductivity was calculated from measurements of density( $\rho$ ), DSC heat capacity ( $C_p$ ) and laser flash diffusivity ( $D_T$ ) as detailed in chapter 2. Density was measured to be 6.7 g/cm<sup>3</sup> by geometric calculation and confirmed by principle of Archimedes. Thermal diffusivity decreases linearly from 300 K to 360 K, see Figure 7.3(a). From 360 K to 410 K the thermal diffusivity shows an excellent fit to a critical power law with  $T_c = 410$  K and critical exponent  $r = 0.80$ . Above the 410 K phase transition the thermal diffusivity is again changes only in a steady linear fashion with temperature.

Heat capacity is presented here in Figure 7.3(b), but it was discussed in great detail in section 5.3. Below 360 K and above 425 K the heat capacity gives a baseline value of 0.374 J · g<sup>-1</sup>K<sup>-1</sup>, consistent with the Dulong-Petit  $c_p$  for Cu<sub>2</sub>Se, 0.361 J · g<sup>-1</sup>K<sup>-1</sup>.

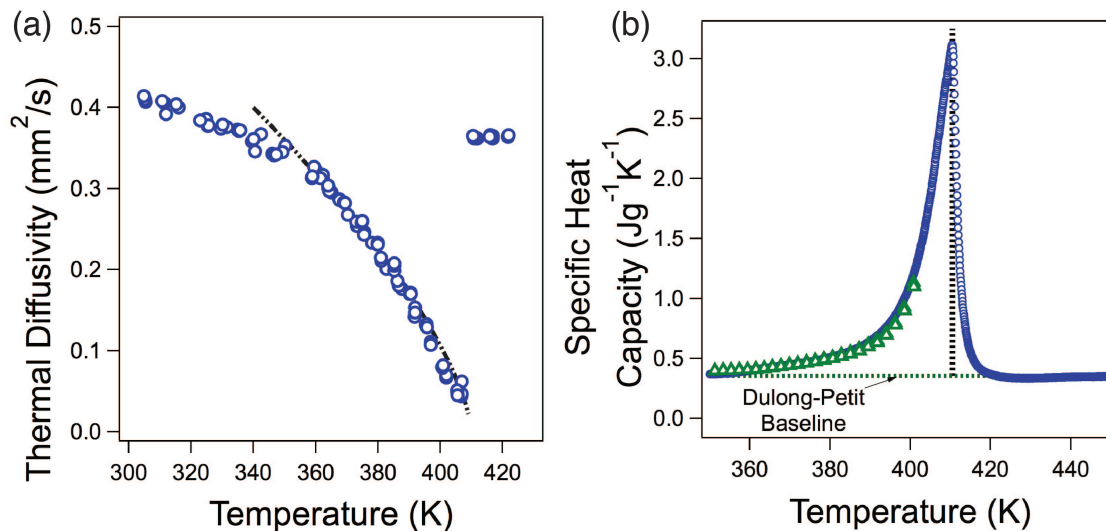


Figure 7.3: Thermal diffusivity (a) and specific heat capacity (b) for  $\text{Cu}_2\text{Se}$  from its room temperature through its 410K phase transition

The 60 K breadth of the peak is indicative of the continuous nature of the transition. In the transition region there is a lambda-type peak, as is characteristic of continuous phase transitions in ionic conductors [118].

From the transport properties described above,  $zT$  was calculated. (Figure 7.4).  $zT$  doubles over a 30 K range peaking at 0.7 at 406 K. Though strong non-linearity in each of the individual transport variables onsets at 360 K, there is no non-linear in  $zT$  until 390 K. This suggests that more than different effects — perhaps associated with the multiple  $\text{Cu}_2\text{Se}$  phase transitions — are needed to explain the anomalous transport behavior between 360 K and 410 K.

### 7.3.1 Analysis

Excepting the region of elevated  $zT$  (390 K to 410 K) all the observed variation in transport can be explained by a simple band structure model. From knowledge of the band structure, the energy dependence of scattering, and the reduced chemical potential, all thermoelectric transport properties can be modeled for typical systems. Though  $\eta$  cannot be easily measured, it can be inferred from the Seebeck coefficient from Equation 6.3. In the degenerate (metallic) limit this dependence can be

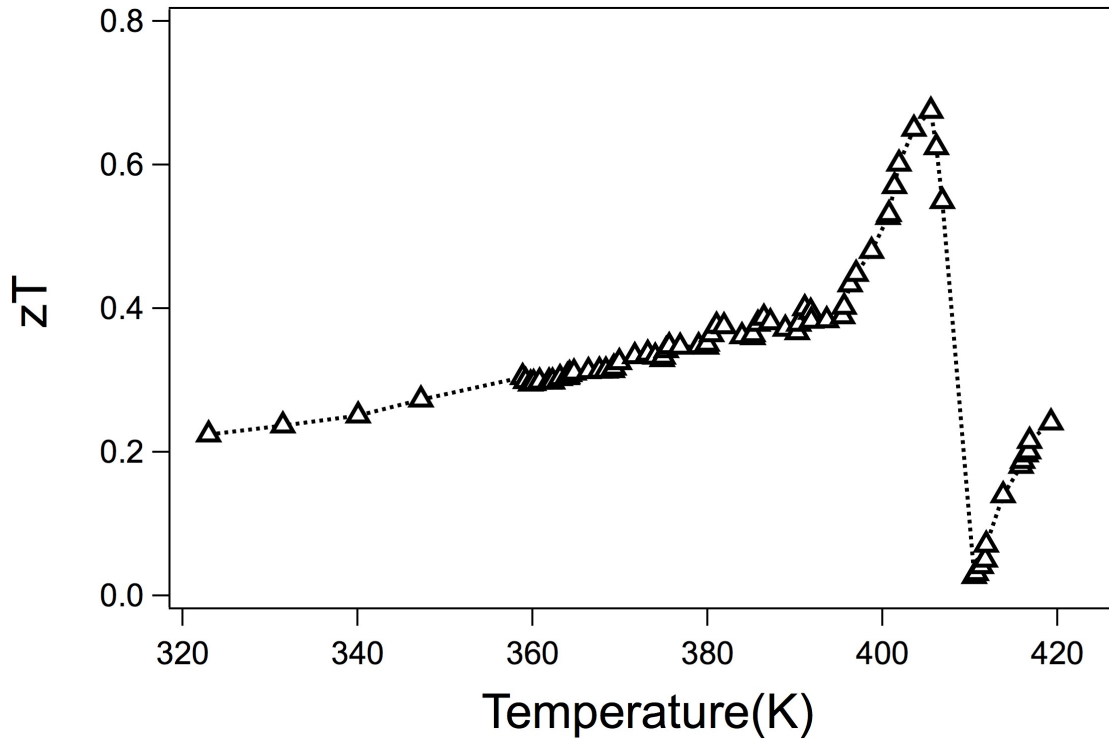


Figure 7.4:  $zT$  for  $\text{Cu}_2\text{Se}$  from its room temperature through its 410 K phase transition.

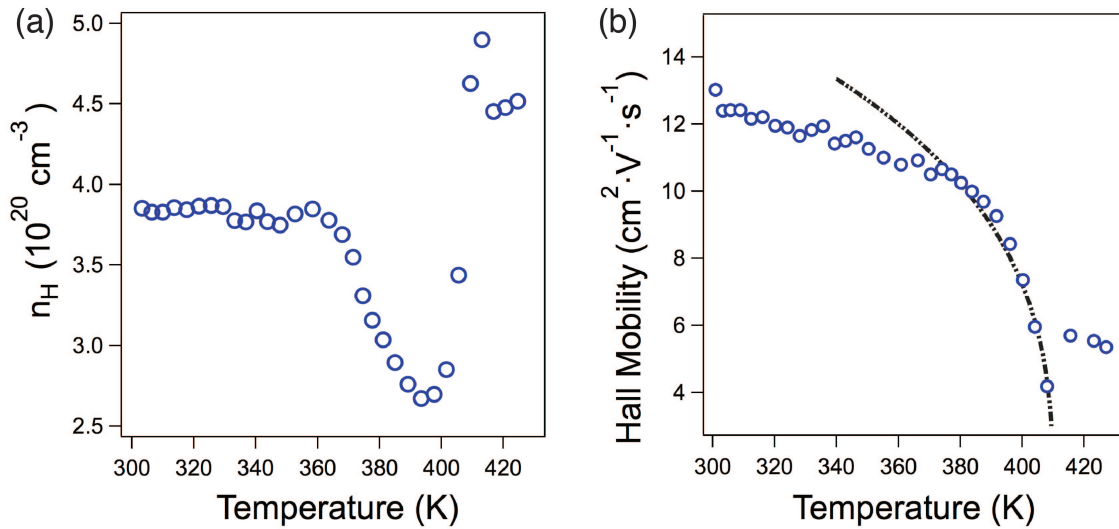


Figure 7.5: Hall Carrier Concentration (a) and Hall Mobility (b) of  $\text{Cu}_2\text{Se}$ . The minimum of  $n_H$  is at 390 K, while  $\mu_H$  decreases until 410 K.  $\mu_H$  could be fit to a power law with critical exponent  $r = 0.32$

expressed in a simple closed form:

$$n = 4\pi \left( \frac{2m^*kT}{h^2} \right)^{3/2} F_{1/2} \quad (7.15)$$

The Hall coefficient ( $R_H$ ) and electrical conductivity were measured via the Van der Pauw method using a 1 Tesla magnetic field at the NASA-JPL thermoelectrics laboratory. From these measurements  $n_H$  and the Hall carrier mobility were extracted, see Figure 7.5. From 300 K to 360 K  $n_H$  is constant while  $\mu_H$  steadily decreases. The linear decrease in  $\sigma$  (Figure 7.2a) observed is entirely due to a decrease in mobility. Given the association with the copper disordering phase transition, it is possible that a scattering mode like the dumb-bell mode of  $\text{Zn}_4\text{Sb}_3$  is steadily activated in this temperature range [173]. Between 360 K and 410 K, the Hall carrier concentration dips until it reaches a minimum of  $2.7 \times 10^{20} \text{ cm}^{-3}$ . This minimum occurs at 393 K, 10 K lower than the minimum in electrical conductivity and the maxima in Seebeck coefficient. This minima is also very close in temperature to where the  $zT$  shows its non-linear increase in temperature, suggesting that the mechanism that causes the increase in  $zT$  also cause the change in trend of  $n_H$ . During this temperature range  $\mu_H$  could be fit to a power law with critical exponent  $r = 0.32$ . The Hall mobility remains low in the high temperature phase — the mobility is 30% below the value expected from extrapolation of low temperature behavior. This is unsurprising given the phonon softening observed in the structurally identical room temperature  $\text{Cu}_{1.8}\text{Se}$  [44].

Equation 7.15 suggests that three factors may cause an anomalous increase in the Seebeck coefficient: a decrease in the carrier concentration ( $n_H$ ), an increase in the scattering parameter ( $\lambda$ ), or an increase in the band effective mass ( $m^*$ ). An increase  $\lambda$  is unlikely. The structural delocalization as presented in our p.d.f. data in section 5.3 may lead to an increase in the intensity of acoustic phonon scattering, but it will not alter that effect's energy dependence. Near a phase transition a low frequency optical phonon mode — a *Goldstone* mode — may be present. However, the energy dependence of optical phonon scattering via lattice deformation is the

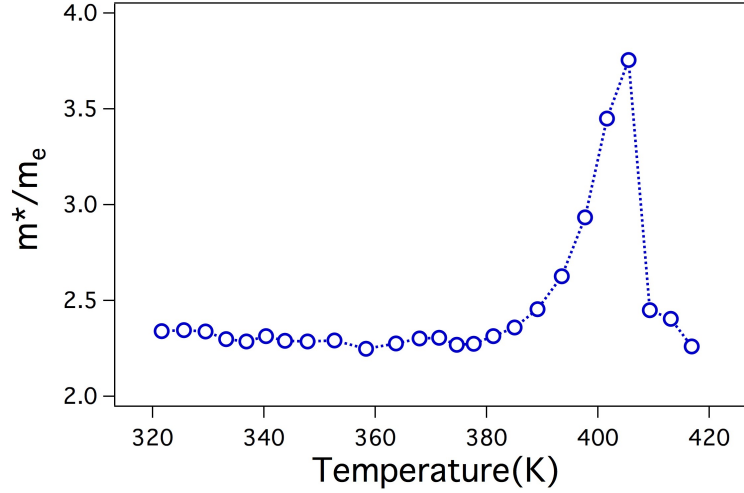


Figure 7.6: Band effective mass need to explain the  $n_H$  and  $\alpha$  data for  $\text{Cu}_2\text{Se}$ . The transient 50% increase in  $m^*$  needed to explain the data is inconsistent with the continuous transformation observed in crystallography.

same as that for electrons and the dependence via dipole effects is only slightly larger than that for acoustic phonons [8].

By modeling with a single parabolic band using measured values of temperature, Seebeck, and  $n_H$ , the shift in  $m^*$  required to explain the data can be calculated, see Figure 7.6. Up to 380K the data can be explained entirely with a SPB with  $m^* = 2.3 m_e$  ( $\pm 5\%$ ). Above this temperature an increase in  $m^*$  of up to 50% is required followed by an even more sudden decrease. This is physically inconsistent with the continuous transformation observed via crystallography, see section 5.3. Effective mass can be related to the band structure at the Fermi level by the formula:

$$m^* = \hbar^2 \left( \frac{\partial^2 E}{\partial k^2} \right)^{-1} \quad (7.16)$$

Equation 7.16 means that a substantial change in  $m^*$  requires a substantial change in the reciprocal space band structure. As the reciprocal space band structure is related by Fourier transformation to the physical spatial representation of the atomic orbitals and thus the coordination of the atoms. A substantial change in  $m^*$  would therefore require a significant change in local electron coordination — a change that is inconsistent with the minor change in band structure seen in temperature-resolve

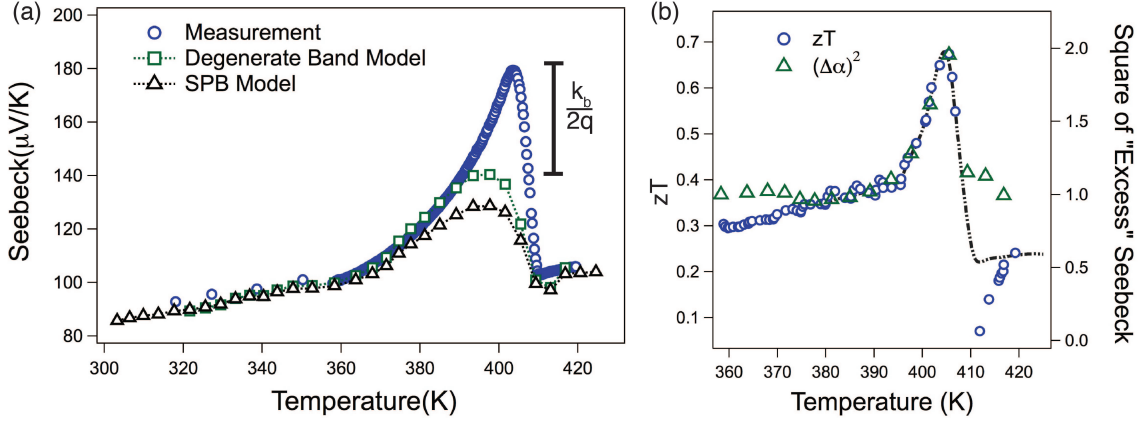


Figure 7.7: Measured Seebeck coefficient compared with predictions from band structure model with  $m^* = 2.3 m_e$  and measured  $n_H$  (a). The square of the Seebeck excess to the band structure prediction (b) explains the  $zT$  peaks size and breadth.

PXRD. It would further require this change to be transient, existing only in proximity to the 410 K. However, the electron bands are dependent on the average structure rather than the correlation length of the order parameter. Thus we expect the effective mass and other band structure attributes should vary smoothly from one phase to the other, rather than peaking at the phase transition.

While the observed shift in carrier concentration cannot explain the peak in Seebeck, it does elucidate one apparent anomaly in the transport data. As discussed in the previous section the onset of non-linear transport behavior occurs at 360 K, but the  $zT$  shows a visible deviation from a linear trend only at 393 K. In Figure 7.6 it is seen that deviation from a constant  $m^*$  begins at 380 K to 385 K. The measured Seebeck coefficient and that predicted by Equation 6.5 and a single parabolic band model with  $m^* = 2.3 m_e$  are compared in Figure 7.7. Near 385 K both models show a increasing deviation from the measured data. This increase is of order of the natural scale of Seebeck,  $k_b/2q = 43 \mu\text{V}/\text{K}$ ; the increase corresponds to transport of the entropy of an additional degree of freedom per electron.

When the square of the measured Seebeck divided by the band structure predicted Seebeck is compared with  $zT$ , as in Figure 7.7b, it is seen that the anomalous increase in Seebeck almost explains the observed breadth and height of the  $zT$  peak. The measured Seebeck is 48% higher than the prediction of the SPB model and 40% higher

than the prediction of the degenerate band model at the temperature of peak  $zT$ , 406 K. The measured  $zT$  is 60% higher at its 406 K peak compared to linear extrapolation from its increase from 360 K to 385 K. The excess Seebeck ( $\Delta\alpha$ ) compared to the band structure slightly overestimates the height of the  $zT$  peak. Both the  $zT$  and  $\Delta\alpha$  are increased noticeably over the exact same temperature range of 393 K to 410 K. This suggests that some aspect of the lambda-type phase transition is increasing the  $zT$  of  $\text{Cu}_2\text{Se}$ .

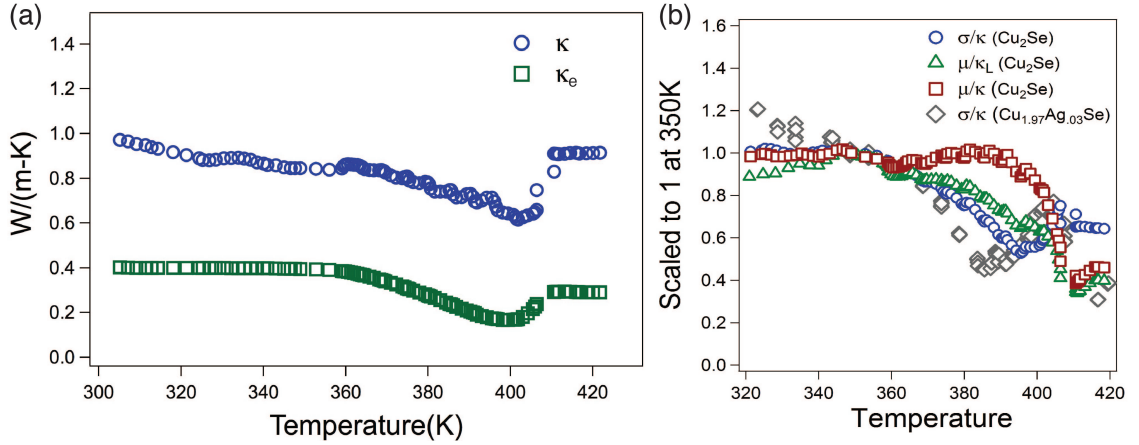


Figure 7.8: Decreasing thermal conductivity does not cause the  $zT$  peak. (a) The decrease in  $\kappa$  is due to the electronic contribution ( $\kappa_e$ ). (b) Electrical properties decrease slower than thermal properties in the phase transition region and thereby diminish the  $zT$  peak.

The  $zT$  increase cannot be explained by a relative improvement of phonon to electron scattering; that is by the  $\sigma/\kappa$  contribution to  $zT$ . While there is insufficient data to truly determine the Lorenz number ( $L$ ) over the entire phase transition region, single temperature estimates bound it between 1.8 and 2.0  $\text{W}\Omega^{-1}\text{K}^2$ . This allows estimation of  $\kappa_e$  by the formula,  $\kappa_e = L\sigma T$ . The estimated electronic portion of the thermal conductivity qualitatively explains the observed decrease in total thermal conductivity, see Figure 7.8(a).

Direct comparison of electron ( $\mu_H, \sigma$ ) and thermal transport ( $\kappa, \kappa_L$ ) indicates that the  $zT$  is not increased by preferential scattering of phonons over electrons, see Figure 7.8(b). Though thermal conductivity decreases between 360 K and 410 K, this decrease is more than counteracted by a decrease in electrical mobility over the same

range. The observed increase in  $zT$  is not due to the reduction of the thermal conductivity via preferential scattering of phonons over electrons. This trend is particularly clear when comparison is made with  $\kappa_L$  instead of  $\kappa$ . This suggests that across the entire temperature range  $\kappa_L$  is close to its glass-like minima, such that further increased scattering from thermally activated modes associated with ion disordering cannot reduce it significantly further. This contradicts the proposal of Liu *et al.* that the increase in  $zT$  is due to preferential scattering of phonons as compared to electrons due to interaction with a soft optical (Goldstone) mode [123].

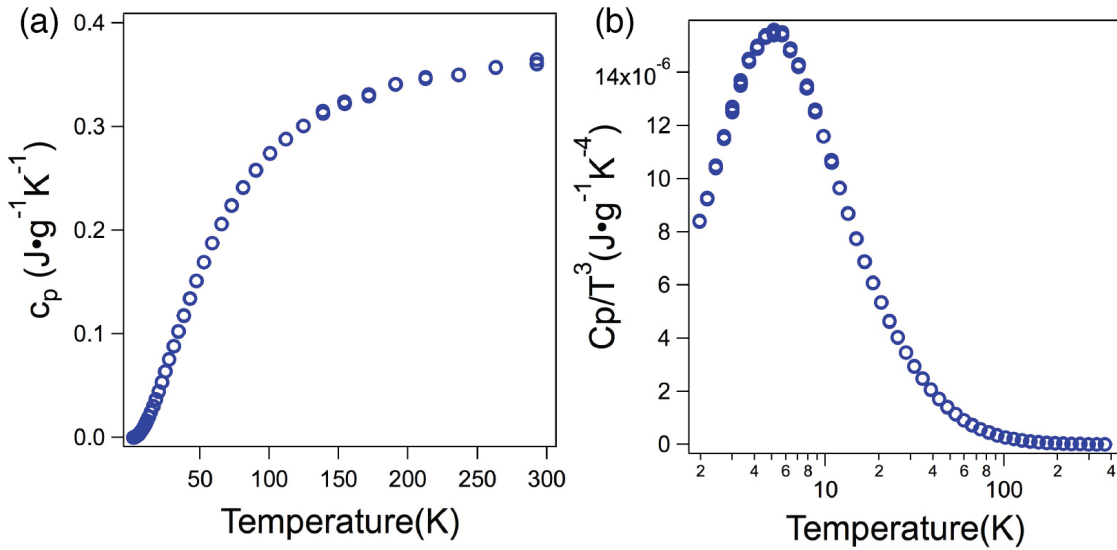


Figure 7.9: Low temperature heat capacity of  $\text{Cu}_2\text{Se}$  (a) indicates an Einstein mode (b) at approx 400 GHz.

It is likely that the measured  $\kappa$  is at or close to its particular glassy limit; this is a major reason for the excellent thermoelectric performance of  $\text{Cu}_2\text{Se}$ . A true glass is characterized by occupation of localized vibrational states instead of extended phonon states. These states will be of relatively low frequency — less than a terahertz — and their occupation will be by the Bose-Einstein distribution:

$$P = \frac{g_i}{e^{hf/k_bT} - 1} \quad (7.17)$$

With resulting heat capacity contribution of:

$$c_V = 3k_b \left( \frac{hf}{k_b T} \right)^2 \frac{e^{hf/k_b T}}{(e^{hf/k_b T} - 1)^2} \quad (7.18)$$

When  $c_V/T^3$  is plotted as a function of  $T$  for a Bose oscillator, it indicates a peak at approximately  $hf = -0.2k_b T$  [98]. This peak is known as a Bose peak and it is characteristic of glassy behavior. A similar feature was observed in the heat capacity of low-temperature  $Zn_4Sb_3$ . That feature was successfully associated with phonon softening and that material's low thermal conductivity [173]. Analysis of low temperature heat capacity data shows  $Cu_2Se$  to have a pronounced Boson peak at 4 K, see Figure 7.9. This suggests a vibrational mode at 400 Gigahertz, and it is strongly indicative of glassy behavior.

We observed a  $zT$  peak concurrent with the lambda-type phase transition in  $Cu_2Se$ . Simultaneously, there is a dramatic increase in thermopower which cannot be explained in terms of a single parabolic band model using the measured Hall carrier concentration and transport data. Transport parameters are strongly affected by the continuous phase transition, with Hall mobility and thermal diffusivity in particular clearly following a critical power law, and the heat capacity showing a characteristic lambda shape. This behavior strongly suggests that  $Cu_2Se$ 's phase transition  $zT$  peak is driven by entropy co-transport.

## 7.4 $Cu_{1.97}Ag_{0.03}Se$

In the prior section I explored how at the phase transition the figure-of-merit of  $Cu_2Se$  can be measured and a strong enhancement shown. However, it is unlikely that  $Cu_2Se$  is the ideal thermoelectric material of its class. In synthesizing the samples no care was given to the stoichiometry or the grain structuring. In fact, the source of the intrinsic high carrier concentration we observed in  $Cu_2Se$ , see Figure 7.5(a), remains a mystery. And though our understanding of the mechanism behind  $Cu_2Se$  phase transition performance is incomplete, we hope that by examining materials with

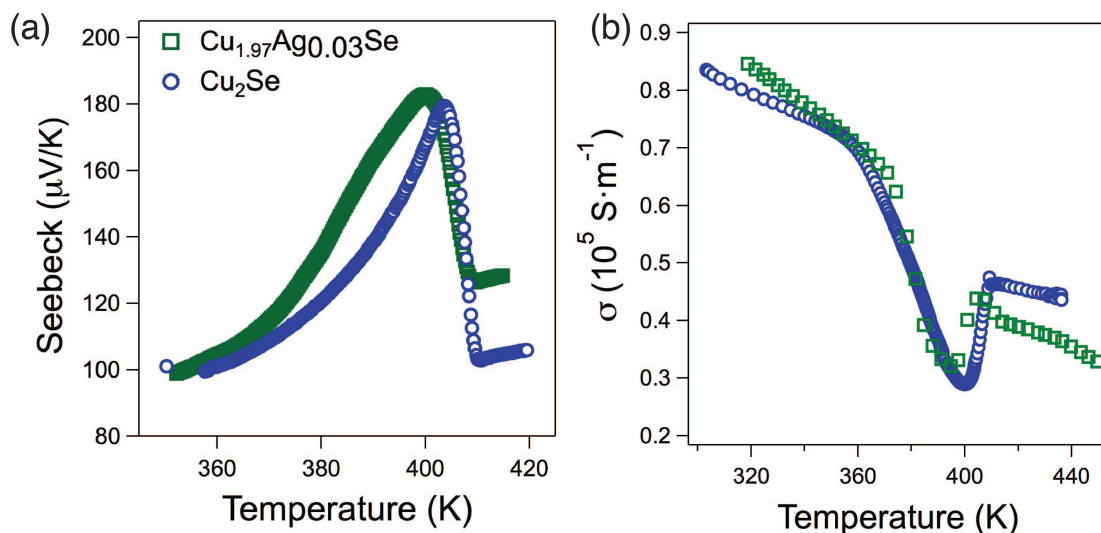


Figure 7.10: Comparison of Electrical Conductivity (a) and Seebeck (b) of  $\text{Cu}_{1.97}\text{Ag}_{0.03}\text{Se}$  with  $\text{Cu}_2\text{Se}$ .

similar compositions that these properties may be expanded upon. Unfortunately, substituting a different element for the copper or the selenium may lead to secondary phase formation; the dissolution of these secondary phases — perhaps more soluble in  $\alpha - \text{Cu}_2\text{Se}$  — may alter the nature of the phase transition and thereby destroy the effect in question of this study.

An interesting case is that of  $\text{Cu}_{1.97}\text{Ag}_{0.03}\text{Se}$ . In Chapter 5, section 5.4 I examined its structural phase transition through temperature-resolved PXR. I determined it to show both a first order transition at 403K, slightly lower than of  $\text{Cu}_2\text{Se}$ , but also to show a similar peak evolution as  $\text{Cu}_2\text{Se}$  below 380 K. At 380 K the secondary phase of  $\text{CuAgSe}$  dissolves, and while some peaks change with the  $\text{Cu}_2\text{Se}$  trend until the first order phase transitions, others showed quite different behavior. There are a few other peaks which slowly diminish to the phase transition temperature; it is unclear if they are an unidentified impurity or additional peaks of a main phase that is slightly different from  $\text{Cu}_2\text{Se}$ .

The transport properties of  $\text{Cu}_{1.97}\text{Ag}_{0.03}\text{Se}$  were measured via the same methods as those described for  $\text{Cu}_2\text{Se}$  in section 7.3 as well as in the chapters on experimental methodology (Chapter 2) and Seebeck metrology techniques (Chapter 3). For the sake

of comparison I plot the data for  $\text{Cu}_2\text{Se}$  and  $\text{Cu}_{1.97}\text{Ag}_{0.03}\text{Se}$  together.

The electrical conductivity of  $\text{Cu}_{1.97}\text{Ag}_{0.03}\text{Se}$ , see Figure 7.10(a), is visually similar to that of  $\text{Cu}_2\text{Se}$ , showing all three characteristic features: a knee at 370 K, a minimum at 395 K, and a kink at 403 K. All three of these features occur at slightly different temperatures for the two samples. The decrease in temperature for the kink corresponds to the sudden first order transition observed. The slope of the conductivity below the knee at 370 K does not follow the power law described by Vucic; the temperature his empirical model predicts for  $\text{Cu}_2\text{Se}$  is 270 K. The concavity of the conductivity of  $\text{Cu}_{1.97}\text{Ag}_{0.03}\text{Se}$  changes sign near 380 K, coincident with the dissolution of the  $\text{CuAgSe}$  secondary phase into the matrix.

While the value of electrical conductivity is similar for both compositions in the phase transition range, the Seebeck of  $\text{Cu}_{1.97}\text{Ag}_{0.03}\text{Se}$ , see Figure 7.10(b), is markedly higher than that of  $\text{Cu}_2\text{Se}$  from 370 K to 400 K. In its increase it is broadened and shows an inhomogeneous shape. While its increase compared to  $\text{Cu}_2\text{Se}$  from 370 K to 380 K is correlated with the faster decrease in electrical conductivity, the increase and broadening above that temperature are likely due to the complicated interaction of the dissolved Ag with the  $\text{Cu}_2\text{Se}$  main phase. Above the phase transition, the Seebeck coefficient of  $\text{Cu}_2\text{Se}$  is slightly higher than of  $\text{Cu}_{1.97}\text{Ag}_{0.03}\text{Se}$ , but the electrical conductivity is correspondingly lower.

Comparison of the thermal properties of  $\text{Cu}_{1.97}\text{Ag}_{0.03}\text{Se}$  and  $\text{Cu}_2\text{Se}$  are particularly illustrative. Just as in  $\text{Cu}_2\text{Se}$  the region of decreasing slope in  $\sigma$  matches a corresponding region in the thermal diffusivity, see Figure 7.11(a). The diffusivity decrease in  $\text{Cu}_{1.97}\text{Ag}_{0.03}\text{Se}$  from 320 K to 360 K is much less than that in the same temperature range for  $\text{Cu}_2\text{Se}$ . Most notably there are two distinct minima in the diffusivity. The minima at 385 K resembles a critical power law decrease, as seen at the 410 K phase transition of  $\text{Cu}_2\text{Se}$ . Between 390 K and 410 K there is a steady decrease in the diffusivity, suggesting that the dissolution of the secondary phases is broadening out the phase transition region. As expected the phase transition temperature in thermal diffusivity occurs at a lower temperature for  $\text{Cu}_{1.97}\text{Ag}_{0.03}\text{Se}$  than for  $\text{Cu}_2\text{Se}$ . In the high temperature phase  $D_T$  for  $\text{Cu}_2\text{Se}$  is slightly higher than that

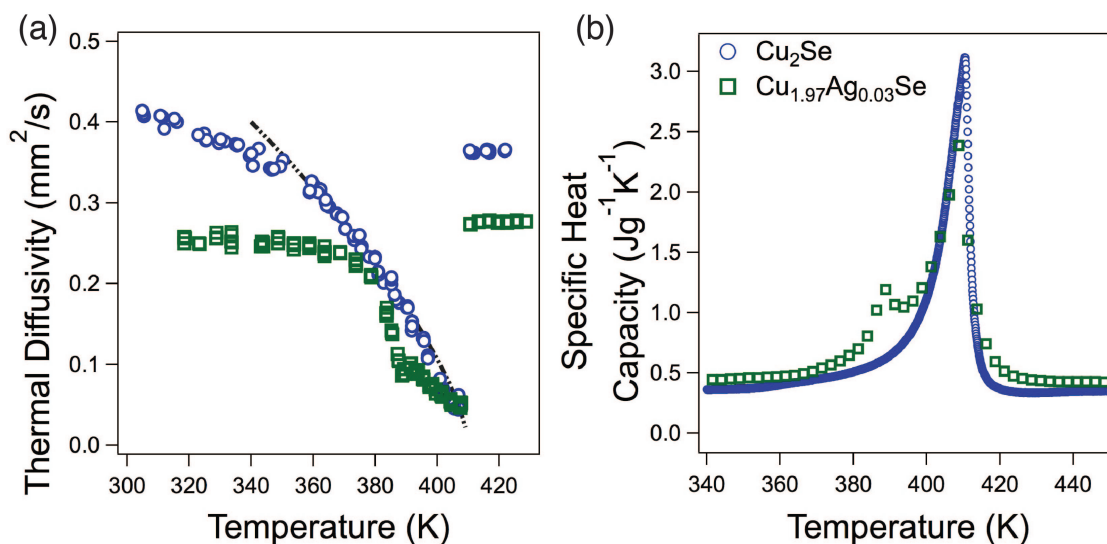


Figure 7.11: Comparison of  $D_t$  (a) and  $C_p$  (b) of  $\text{Cu}_{1.97}\text{Ag}_{0.03}\text{Se}$  with  $\text{Cu}_2\text{Se}$ .

of  $\text{Cu}_{1.97}\text{Ag}_{0.03}\text{Se}$ . As this difference is similar to that of  $\text{Cu}_2\text{Se}$ , it is probably driven by a corresponding decrease in electronic thermal conductivity.

The double minima in  $D_T$  corresponds to a doubled peak in  $c_p$ , see Figure 7.11(b). The heat capacity baseline of  $\text{Cu}_{1.97}\text{Ag}_{0.03}\text{Se}$  is slightly higher than that of  $\text{Cu}_2\text{Se}$  —  $0.42 \text{ J/gK}$  as compared to  $0.37 \text{ J/gK}$ . As the compositions are nearly identical, the Dulong-Petit heat capacity should be nearly the same, so this difference is due to systematic measurement error or from a higher coefficient of thermal expansion. The heat capacity from 320 K to 360 K is greater than the high temperature baseline, and it shows a linear increasing trend. At 360 K there is a kink in the heat capacity above which the data is non-linear. This kink exactly mirrors that seen in  $\text{Cu}_2\text{Se}$ , suggesting that though the middle temperature second order transition is more difficult to observe in  $\text{Cu}_{1.97}\text{Ag}_{0.03}\text{Se}$  than  $\text{Cu}_2\text{Se}$ , it is a feature of both systems. The 403 K peak, representing in part a first order transition, must include a discrete enthalpy of formation. As I cannot determine which portion of the DSC curve is due to the enthalpy release of a first order phase transition, I treat all of it as a portion of the specific heat capacity. This will result in an unknown underestimate of the  $zT$  between 400 K and 420 K.

The  $zT$  of  $\text{Cu}_{1.97}\text{Ag}_{0.03}\text{Se}$  dwarfs that of  $\text{Cu}_2\text{Se}$ , reaching a maximum of 0.95 at

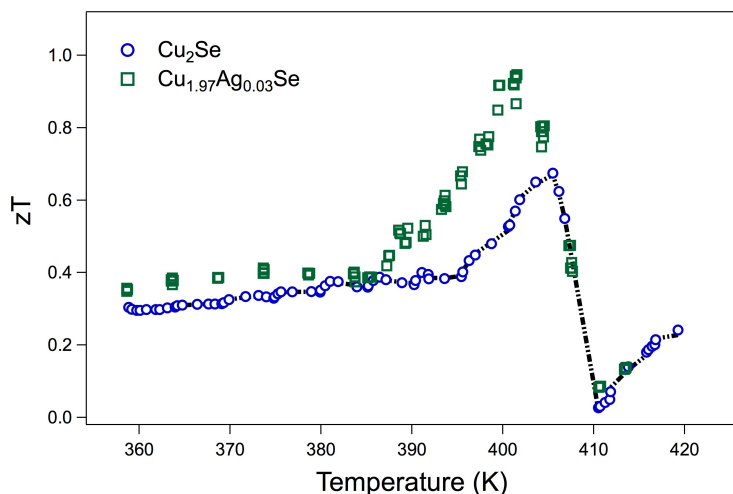


Figure 7.12: Comparison of  $zT$  of  $\text{Cu}_{1.97}\text{Ag}_{0.03}\text{Se}$  with  $\text{Cu}_2\text{Se}$ .

402 K, see Figure 7.12. The maximum  $zT$  is reached just prior to the 1st order phase transition temperature. The  $zT$  shows a kink at 385 K, corresponding to the temperature of the secondary diffusivity minima and heat capacity peak as well as the dissolution of the  $\text{CuAgSe}$  phase. This is the same temperature at which the measured Seebeck for  $\text{Cu}_2\text{Se}$  begins to exceed the value predicted by the single parabolic band. This correlation may be causal. The disordering of the main phase may decrease the chemical potential for additional Ag or Cu to be added to it. By doing so it may instigate the dissolution.

Band structure analysis could not be performed on  $\text{Cu}_{1.97}\text{Ag}_{0.03}\text{Se}$  due to bipolar effects from the secondary phase of  $\text{CuAgSe}$ . Measurements of Hall coefficient in the low temperature phase (Figure 7.13(a)) show it to be negative. For a single band thermoelectric the Hall coefficient and the Seebeck should have the same sign — that of the majority carrier. As discussed in detail in chapter 2, the effect of a minority carrier band is linear with its mobility in Seebeck but quadratic in the Hall coefficient. The  $\text{CuAgSe}$  secondary phase high mobility n-type bands with mobility of order  $10^4 \text{ cm}^2/\text{V} \cdot \text{S}$  [88]. As a band's Hall coefficient characteristic field is the inverse of its field, this indicates a transformation from electron to hole dominated behavior should occur in the 1 to 10 T range.

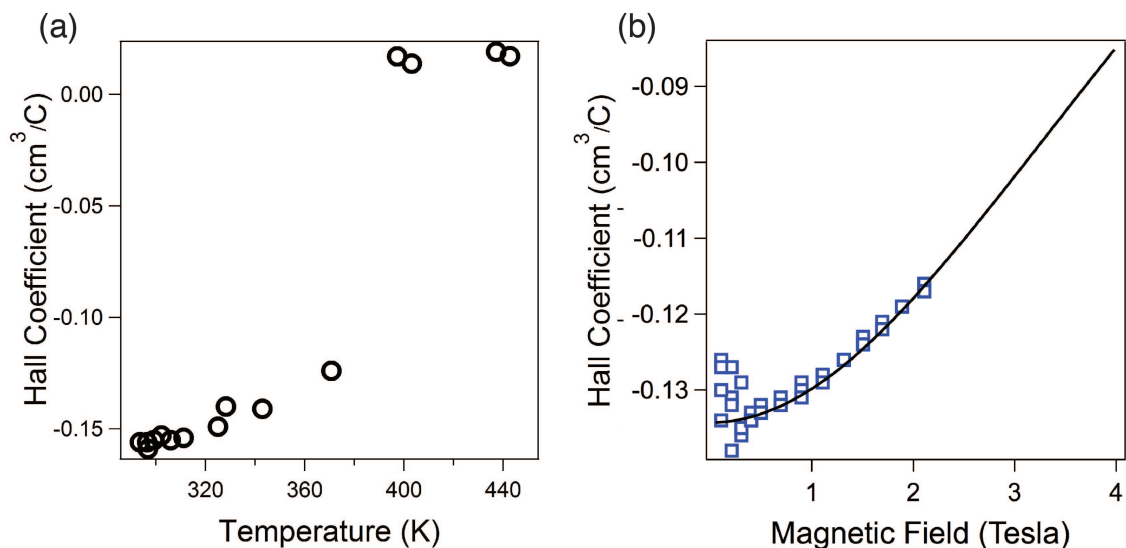


Figure 7.13: Hall coefficient for  $\text{Cu}_{1.97}\text{Ag}_{0.03}\text{Se}$  at 2 T and varying temperature (a) and at 293 K with varying magnetic field.

The Hall coefficient was measured under magnetic fields varying from 0.1 T to 2.2 T in steps of 0.1 T below 1 T and in steps of 0.2 T above it. Though low field measurements were below the noise floor, data above 0.3 T showed a clear increasing trend, see Figure 7.13(b). This trend is consistent with two single carrier bands with  $n = 1 \times 10^{17} \text{ cm}^{-3}$ ,  $\mu_n = 1440 \text{ cm}^2\text{V}^{-1}\text{s}^{-1}$ ,  $p = 4 \times 10^{20} \text{ cm}^{-3}$ , and  $\mu_p = 11 \text{ cm}^2\text{V}^{-1}\text{s}^{-1}$ . The p-type characteristics were chosen to be similar to that of  $\text{Cu}_2\text{Se}$  and the n-type parameters adjusted until a visual fit could be made. This fit is shown as a black line in Figure 7.13(b).

When examining the transport properties near a phase transition, it is of utmost importance to verify that they are stable. When measuring the Seebeck coefficient via the ramp method, half of the data used was measured while the average sample temperature was increasing (on heating), and half the data was measured while the average sample temperature was decreasing (on cooling). From all of the voltage  $\Delta T$  points measured at a given temperature, the Seebeck data shown in Figure 7.10 were determined. If the phase transitions are interfering with the transport properties, this should be visible in a difference between the Seebeck of the data from heating and cooling.

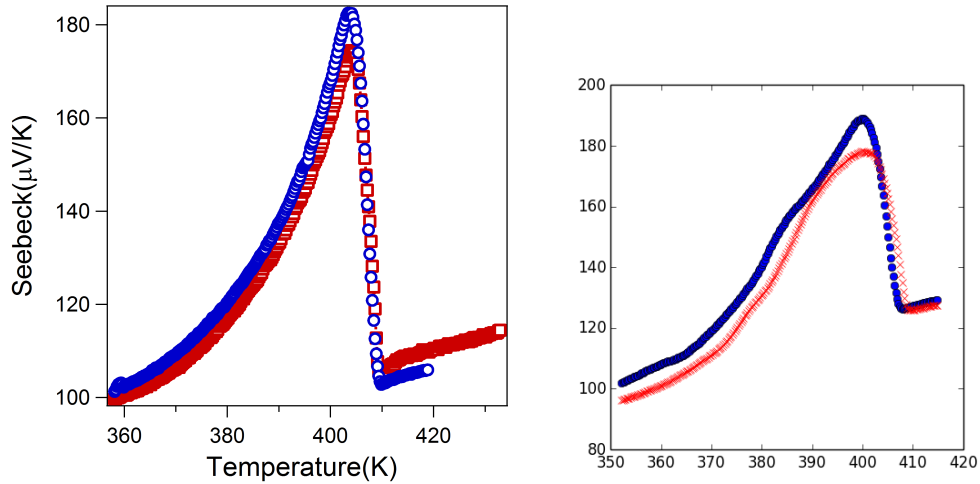


Figure 7.14: Ramp Seebeck fits for the cooling data (blue) and heating data (red) separately in  $\text{Cu}_2\text{Se}$  (a) and  $\text{Cu}_{1.97}\text{Ag}_{0.03}\text{Se}$  (b)

The ramp method Seebeck determined for both the heating and cooling data is shown in Figure 7.14(a) for  $\text{Cu}_2\text{Se}$  and in Figure 7.14(b) for  $\text{Cu}_{1.97}\text{Ag}_{0.03}\text{Se}$ . The data for  $\text{Cu}_2\text{Se}$  shows an offset of less than 5% between heating and cooling across the temperature range. The value at the 406 K  $zT$  peak is identical on both heating and cooling. The average value is midway between the heating and cooling curves. The differences between the curves are within systematic measurement uncertainty; they are probably due to a slight alteration in thermal contact resistance on heating and on cooling.

The data for  $\text{Cu}_{1.97}\text{Ag}_{0.03}\text{Se}$  shows values that are within 10% on heating and cooling, other than in the small temperature range above the 403 K phase transition. A small hysteresis in the data is observed. The line shapes of the curve are slightly different. The average Seebeck shown in Figure 7.14(b) is much closer to the data measured on heating than that measured on cooling. This suggests that the visually notable 5% discrepancy in the data at 400 K is driven by greater noise in the data on cooling than on heating. Another possibility is that there is a longer time-scale required for precipitation of an impurity phase than there is for its dissolution at the 403 K phase transition. The discrepant range corresponds to the temperatures between the first order phase transition and the dissolution of the  $\text{CuAgSe}$  secondary

phase. The precipitation and dissolution of the CuAgSe phase may increase the kinetics of secondary phase restructuring.

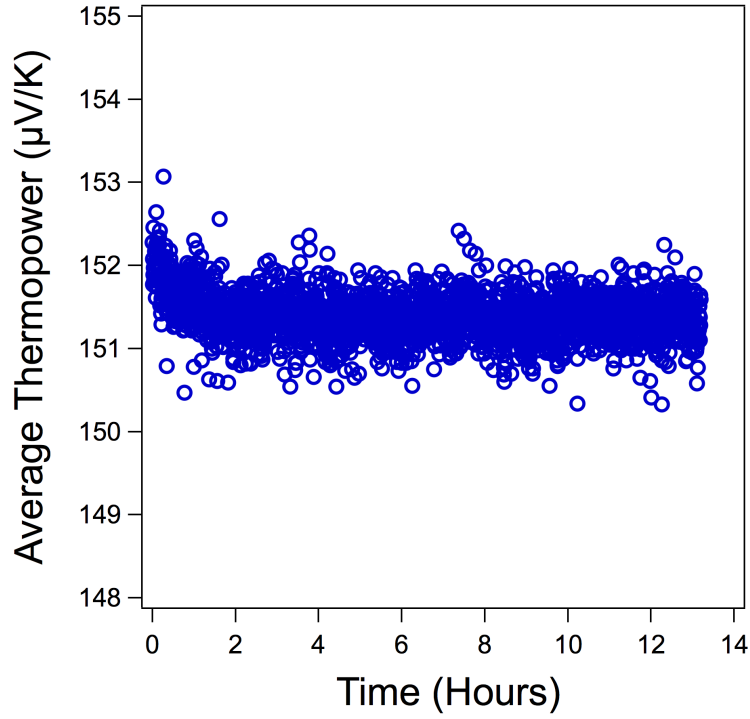


Figure 7.15: Measured Seebeck voltage of Cu<sub>2</sub>Se at  $\bar{T} = 390$  K and  $\Delta T = 16$  K. There was a variation of less than 1% in the measured values. After the temperature gradient stabilized there was no variation.

The Seebeck coefficient of Cu<sub>2</sub>Se just below its phase transition temperature is very stable, indicating it is a steady state property of the material, see Figure 7.15. The sample was held at an average temperature of 390 K and a temperature difference of 16 K for 13 hours. The measured thermopower, 152  $\mu\text{V}/\text{K}$ , varied by less than 1% during this time period. The predicted average thermopower for this range was calculated by integration of the data shown in Figure 7.2(a) as 143  $\mu\text{V}/\text{K}$ . This 6% discrepancy between the predicted and measured value is consistent with the repetition error of Seebeck measurements. As the discrepancy would suggest that Seebeck and  $zT$  are underestimated, it does not undermine the conclusion of phase transition enhanced thermopower.

In the next and concluding chapter I will summarize the experimental results in the context of super-ionic phase transitions. I will present a suggestion for how the

data for  $\text{Ag}_2\text{Se}$  and  $\text{Cu}_2\text{Se}$  may be explained based on the irreversible thermodynamics of phase transitions.